7

Fourier Transform Infrared Microspectroscopy for Cancer Diagnostic of C6 Glioma on Animal Model

Beljebbar A. and Manfait M.
Unité MéDIAN, MEDyC, CNRS UMR 6237, IFR 53, UFR de Pharmacie, Université de Reims Champagne-Ardenne France

1. Introduction

Cancer is one of the leading causes of death in the world. Currently, the gold standard in most cancer diagnosis is histopathological evaluation, which involves the removal of tissue biopsies and examination by pathologists. This process includes tissue staining and morphological pattern recognition. During tissue transformation, it is expected that substantial modifications occur at molecular level before visible morphological changes become apparent. Histological examination requires extensive human observations to recognize both the constitutive histologic entities and the pathologic state. Early detection of cancer is the most important factor in the prevention of cancer and a guarantee in most cases of an effective treatment and in some cases for a complete cure. Moreover, the histological assessment must be performed while surgery is ongoing to determine whether the tissue has been removed or spared. For example, brain tissue cannot be removed with a large safety distance from the tumor. The resection of brain tumors is strongly limited to the border of the tumor. The main objective is a detection of the source of the pathological variation at molecular level in order to further understand the molecular carcinogenic process in a range of cancers. Indeed, tumor tissues are mostly heterogeneous in nature, and this heterogeneity further depends on the stage of disease and its aggressiveness. The emergence of a novel technique, complementary to histopathology and immunohistochemistry, can thus help in the early diagnostic of tissue transformation during carcinogenesis.

Fourier-transform infrared microspectroscopy (FTIRM) has emerged as a powerful tool to study molecular structure and structural interactions in biological systems. When this technique is applied to tissues, the resulting spectra is composed of characteristic absorption bands originating from all infrared-active vibrational modes of biological macromolecules present in the tissue, such as proteins, lipids, and nucleic acids (Parker, 1971). Each of these molecules provides a unique absorption spectral pattern named fingerprint through the entire infrared spectrum. This property offers a way to identify the molecule type (qualitative analysis) and the amount or quantity of this molecule in the sample (quantitative analysis) (beljebbar et al., 2008). This method can be used as a diagnostic tool, complementary to histopathology or immunochemistry (Fernandez et al., 2005). As the

image contrast is based on the intrinsic vibrational signature of the tissue components, spectral images does not require the use of added dyes or labelling methods for visualization of different chemical components in the sample (Bates, 1976). Indeed, FT-IRM imaging combined a high spatially resolved morphological and biochemical information that offer a number of advantages for ex-vivo assessment of tissue and aid the histopathologist in the identification and classification of subtle biochemical changes related to carcinogenesis (Petibois & Déléris, 2006; Cohenford & Rigas, 1998; Kneipp et al., 2000; Yano et al., 2000). With the fast image acquisition provided by modern mid-infrared imaging systems, it is now envisaged to analyze tumor biopsies in delays compatible with surgery (Levin & Bhargava, 2005). Other advantages of this method are that it is objective and provides reproducible diagnosis, minimize inter-observer variability. Indeed, IR spectroscopy can detect and monitor characteristic changes in molecular composition and structure that accompany transformation from normal to cancerous state (Afanasyeva et al., 1998, Diem et al., 1999, Franck et al., 1998). The identification and quantification of these specific molecular changes within tissues can provide diagnostic information for aiding in early detection of diseases and their optimized treatment. Correlations of morphologic and biochemical tissue differences could be used to identify variations that occur between healthy and diseased tissues. The development of clinical protocols for the routine examination of tissue histology or of localized tumors using IR microspectroscopic methods has been largely used in medical diagnostics to identify neoplasia in breast, (Ci et al, 1999) cervix, (Wong et al, 1991) colon, (Rigas et al, 1990) lung, (Yano et al, 2000) stomach, (Li et al., 2005) and glioma. (Krafft , 2006, 2007; Amharref et al, 2006; Beljebbar et al., 2008).

Infrared spectra contain many overlapping bands and so data interpretation cannot be made by simple visual inspection and alternative approaches are needed. Because of the high complexity of the FTIR spectra obtained from tissues, multivariate statistical methods are required to extract biochemical information related to tissue. This would permit to objectively differentiate distinct tissue structures and for identifying origin that gave rise to the specific tissue pathology. These methods have had a major impact on the quantitative and qualitative analysis of infrared spectral data. They have been shown to improve analysis precision, accuracy, reliability, and applicability for infrared spectral analyses relative to the more conventional univariate methods of data analysis. Rather than attempting to find and use only an isolated spectral feature in the analysis of spectral data, multivariate methods derive their power from the simultaneous use of multiple intensities (i.e. multiple variables) in each spectrum (Mourant, et al., 2003). During the last decade, it has been recognized that FT-IR, in combination with the appropriate multivariate analysis strategies, has considerable potential as a metabolic fingerprinting tool for the rapid detection and diagnosis of disease or dysfunction (Goodacre et al, 2004; Diem et al., 1999). Multivariate imaging techniques including Unsupervised Hierarchical Cluster Analysis (UHCA) (Jackson et al., 1998; Mohlenhoff et al., 2005), K-means clustering (Lasch et al., 2004; Zhang et al., 2003), Principal Components Analysis (PCA) (Lasch and Naumann, 1998), Linear Discriminant Analysis (LDA) (Mansfield et al, 1999), Fuzzy C-means clustering (Lasch et al., 2004; Mansfield et al., 1997) and neural networks (Lasch & Naumann, 1998) have proven to be invaluable in the identification of spectral groups or "clusters" which can be directly compared to stained tissue sections. In multivariate methods, the information of the entire spectrum can be utilized for the analysis. The high correlation of spectral clusters with anatomical and histopathological features has been conclusively demonstrated for a number of different tissue types including.

The aim of this chapter was the monitoring and interpretation of molecular changes associated to C6 glioma growth and invasion by micro-FTIR imaging. Micro-FTIR maps were recorded on normal brain tissue and on glioma growth after injection of C6 glioma cell suspension in brain parenchyma. Multivariate statistical analysis were used to i) identify the molecular changes associated with the development of the glioma tumor ii) definition of the tumor and peritumoral margins, iii) grading of malignancy and prognosis based on the presence of necrosis. We have investigated the spatial distribution of molecular changes associated with C6 glioma progression using integrated intensity ratios of some specific bands associated to lipids and proteins in order to determine spectroscopic markers to successfully monitor the changes in the molecular composition associated to C6 glioma progression.

2. FTIR characterization of normal brain tissues and C6 glioma progression using cluster analysis

To investigate the potential of FTIR spectroscopy for clinical application, experimental animals are necessary. Rat C6 glioma cells are an experimental cell line that when injected into neonatal Wistar rats grow into an intracerebral tumor with pathological similarities to human glioblastoma (GBM) (Auer et al., 1981). This glioblastoma model was used in a variety of studies related to brain tumor biology including tumor growth (Nagano et al., 1993; San-Galli et al., 1989), invasion (Nagano et al., 1993; Bernstein et al., 1991; Chicoine & Silbergeld, 1995), and evaluation of the therapeutic efficacy of cancer treatments (Barth 1998). The glioma tumors were obtained by injection of C6 glioma cells suspension in brain parenchyma as described elsewhere (Grobben et al., 2002). All animals with implanted C6 cells developed tumors with reproducible localization and size around the site of injection. These groups were sacrificed after 5, 7, 9, 12, 15, 19, days post-implantation (PI). After brain excision, tissue samples were snap-frozen by immersion in methyl-butane cooled down in liquid nitrogen and stored at - 80°C. Two adjacent sections were cut from each sample using a cryomicrotome. One section, 10 µm thick, was placed onto infrared transparent calcium fluoride (CaF_2) slides for infrared imaging. The second section, 7 µm thick, was placed on a microscope glass slide and stained with hematoxylin and eosin (H&E) for histopathological image. Spectra were collected using an FTIR imaging system (SPOTLIGHT, Perkin-Elmer, France) coupled to a FTIR spectrometer (Spectrum 300, Perkin-Elmer, France). This system is equipped with a liquid N_2 cooled Mercury-Cadmium-Telluride MCT line detector comprised of 16 pixel elements. The microscope was equipped with a movable, software-controlled x, y stage. In this study, FTIR images were collected from selected sites with a spatial resolution of 25 µm/pixel, in transmission mode, in the 4000–720 cm^{-1} range, with a final spectral resolution of 4 cm^{-1}, and 16 scans per pixel. After atmospheric correction, data were cut to high wavenumber fingerprint region (2600 to 3700 cm^{-1}), converted to their first derivative, and smoothed using a seven point Savitzky-Golay algorithm in order to minimise the influence of background scatter in the spectra (Savitzky & Golay, 1964). The resulting spectra were then normalized using a Standard Normal Variate (SNV) procedure. A multivariate statistical analysis (Principal Component Analysis (PCA) and K-Means (KM)) was performed on this dataset. K-means clustering was performed on these principal component scores. Pseudo-color maps based on cluster analysis were then constructed by assigning a color to each spectral cluster. The cluster spectra were calculated by averaging absorbance spectra associated to each group and used for the interpretation of the chemical

or biochemical differences between clusters. All data measured on normal brain and tumor development (from 7 to 21 days growth) were pooled in one dataset, processed at the same time and the results were displayed as pseudo-color maps with the same color scale. In this way, we can easily determine all their common and discriminating features by comparing their infrared maps. The rat brains analysed before 5 days after tumor implantation did not show any visible changes in the brain tissue (data not shown). Indeed, all animals died beyond 25 days post-implantation and therefore no data are available beyond this time point.

Histological and FTIR analysis revealed that the tumor size dependent on the period elapsed after injection of glioma cells. Fig. 1 displays FTIR pseudo-color maps of brain tissue and their histopathological images. 13 clusters describing both normal brain and cancer features were extracted and pseudo FTIR maps were constructed with the same color scale. Different clusters in the FTIR images were correlated with features of the histopathological images. White color represents the area where no tissue was present. In the pseudo-color map obtained from glioma tumor obtained 7 days after C6 cells injection (fig. 1B). This pseudo-color map displays some normal structures associated to white matter and grey matter. Cluster 4 described white matter corresponding to corpus callosum (CC) and commissura anterior (CA). CC and CA present important lipid content due to high myelin level in these structures involved in communication within and between hemispheres. Several clusters (6, 1, 2, 8, and 11) describe the transition from white matter to gray matter (cortex). In fact, the CC is the largest white matter structure in the brain, consisting mainly of interhemispheric fibers. Gray matter is distributed at the surface of the cerebral hemispheres (cerebral cortex) and of the cerebellum (cerebellar cortex). It is predominantly composed of neuron cell bodies and unmyelinated axons. Comparison between pseudo-color maps and the histopathology images (Fig. 1A and 1B) shows that the FT-IRM image provides more information on the cortex than standard histopathology. In fact, six layers were identified from the cortex in the pseudocolor FTIR map (fig. 1B), whereas, H&E staining did not allowed to discriminate between these layers in the cortex (fig. 2A). Luxol fast blue (LFB) staining was then used to visualize myelin distribution into brain tissues and to map particular sections within the cortex. In fig. 2B, LFB staining shows a gradation color density between brain structures. In stained preparations, myelin is intensely blue, so that white matter is well differentiated from gray matter. In fact, large fiber tracts like CC and some bundles in CP can be easily recognized. However, even with higher magnification it was very difficult to distinguish between all cortex layers because this staining is mainly restricted to fibers.

Thus, the individual cell type cannot be recognized within the tissue. This LFB staining was then combined with cresyl violet (CV) coloration to stain not only rough endoplasmic reticulum (Nissl substance) but chromatin and nucleoli as well. This coloration was used in our study to visualize all different cell types present in the cortex (Fig. 2C). This pseudo-color FTIR map (fig. 2D) was correlated with that obtained with LFB-CV staining (fig. 2C). With this coloration, six different layers were then identified in the cortex instead of five layers in the FT-IRM map (fig. 2D). On the other hand, when multivariate statistical analysis was applied only on FT-IRM data measured from normal brain tissue we were able to distinguish between five cortex layers. The cortex consists of a thin layer of gray substance which covers the two hemispheres and whose thickness varies between 2 and 4 mm. According to the cortical histological organization, one distinguishes 6 layers numbered from I to VI from top to bottom (Burwell, 2001). The outermost molecular layer (I)

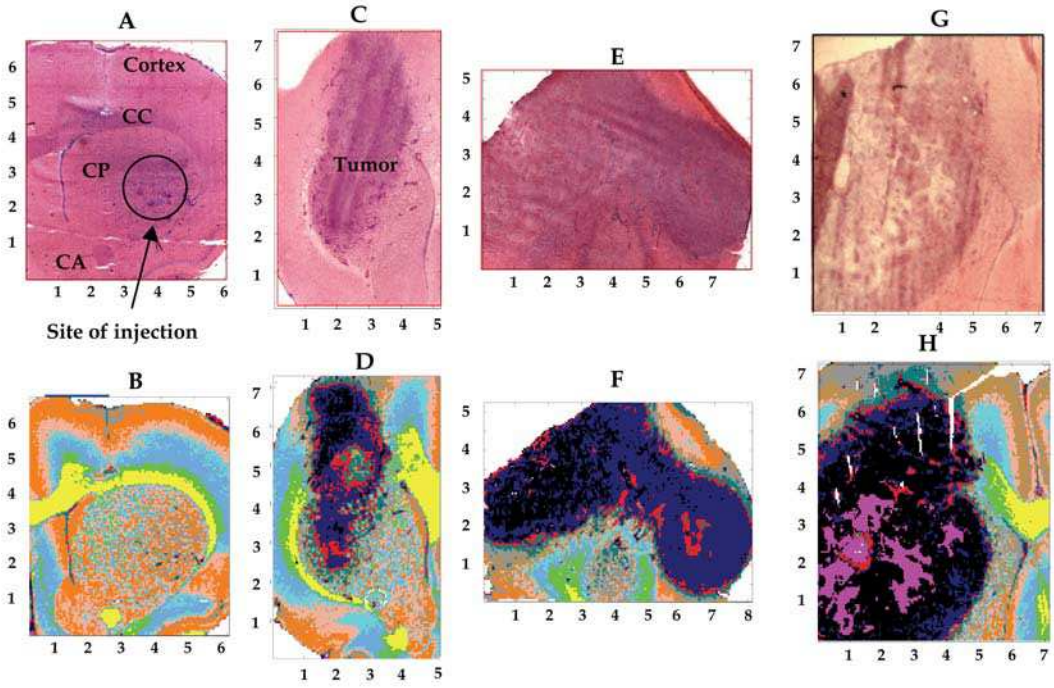

Fig. 1. Photomicrographs (H&E staining) associated to glioma progression (A, C, E, G, I) from respec
days post-implantation. All data measured on several brain tissues during tumor evolution were po
at the same time to extract all features describing both normal and tumor tissues. Data were cut into
3700 cm^{-1}) and cluster analysis was carried out on the first derivative spectra (to enhance the resolut
K-means was calculated the cluster-membership of spectra by assigning each color to one class. Pseu
corresponding histological images were constructed on tumor progression (maps B, D, F, H, and J) r

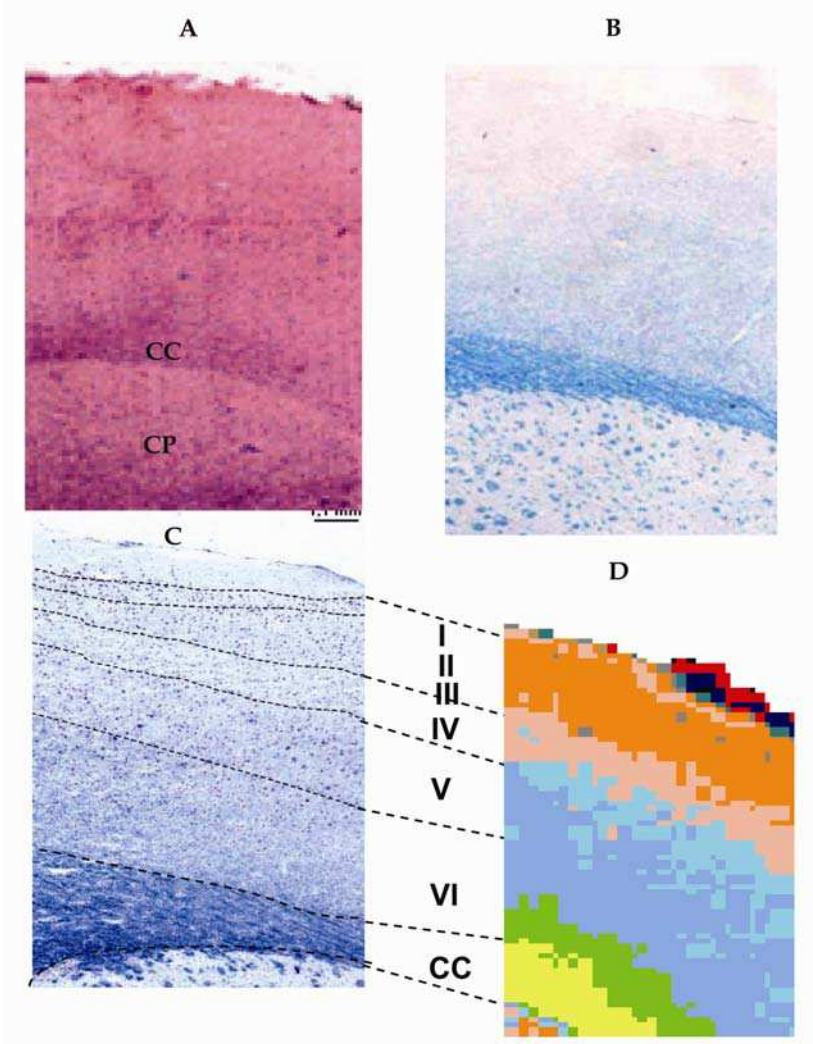

Fig. 2. Photomicrography of a brain tissue section (A) H & E staining, (B) stained with LFB; in this image CC and CP appears more lightly stained, (C) stained with LFB-CV, pointing out the cortical layers of the rat cortex. Pseudo-color FTIR map (D) based on K-means cluster analysis applied only on FTIR data measured from normal brain structures

containing non-specific fibers, corresponds to the yellow cluster. The external granular layer (II) is a rather dense layer composed of small cells. The external pyramidal layer (III) contains pyramidal cells, frequently in row formation. These three layers were encoded by cluster 11. The internal granular layer (IV) is usually a thin layer with cells similar to those in the external granular layer (cluster 8). The ganglionic layer (V) contains, in most areas, pyramidal cells that were fewer in number but larger in size than those in the external pyramidal layer (clusters 1 and 2). The fusiform layer (VI) consists of irregular fusiform cells

whose axons enter the adjacent white matter known as the CC (cluster 1 and 6). By correlating FT-IRM spectral maps with histopathology (H&E, LFB, and LFB-CV) of the adjacent tissue sections, we highlighted the potential of FT-IRM to identify the morphologic origin that gave rise to the specific spectral features found in this study. In fact, with standard staining (H&E), we were not able to discriminate between the different cortex layers. On the other hand, FT-IRM pseudo-color maps were clearly similar to LFB-CV staining for visualizing myelin distribution in healthy brain tissues (white and gray matters).

Fig. 1B exhibit a particular structure (cluster 7) located in the caudate putamen (CP) corresponding to C6 cells injection site. This feature was associated to C6 cell growth. Histological interpretation however showed small abnormalities in rats sacrificed seven days after implantation of C6 cells (fig. 1A). Indeed, this abnormality is characterized by a diffuse structure within the brain parenchyma. The tumor cells appear scattered in the form of cells or grouped in clusters in the vicinity of the blood vessels. At day 9, the viable tumor started to be visible in the implantation site, destroys the corpus callosum and grew into all the cortical layers (fig. 1D). The tumor area was encoded by clusters 12 and 13. On the other hand, clusters 5 and 7 were detected around the tumor. These clusters were associated to the proliferative and invasive character of glioma tumors. In fact, in our previous study, immunohistochemical Ki-67 and MT1-MMP staining were used to visualize the proliferative and invasive activities of glioma and were clearly correlated with the cluster that encoded the surrounding tumor area *(*Amharref et al., 2007). Histopathological staining confirms this FTIR result (fig. 1C), In fact, a Large focus of invasion (6mm) were well separated from the surrounding brain tissue. Tumor was hypercellular with cellular and nuclear pleomorphism and mitotic figures observed. From day 12, the tumor is fairly large and deeply situated within the cortex with massive infiltration into the brain tissue (fig. 1F, 1H, 1J). Most of cerebral cortex is destroyed by tumor tissue. At day 15, we observe the appearance of clusters 9 and 5 associated to the formation of necrosis and perinecrosis (fig. 1H). Histological image displayed oedematous zones as well as zones of necrosis with a pseudopalissading cells (> 8mm) (fig. 1G). Around necrotic zones, tumor shows a large cell density with an increase of the proliferation of endothelial cells and haemorrhagic zones. This necrotic zone increased until day 19 post-implantation (fig. 1J). Cluster 5 observed in the border of the necrotic zone seems to correlate with the pseudopalisading formation. Cluster 9 correlates to the center of the necrosis (full necrosis) of the tumor. The presence of necrosis is important for grading tumors and is often linked to a poorer clinical prognosis (Barker et al., 1996). Indeed, the most characteristic finding of glioblastoma is the necrotic foci surrounded by tumor cells (Kleihues et al., 1993). Pallisading cells delineate the foci of necrosis and lymphocytic infiltration, with the occasional formation of edema fluid (Auer et al., 1981). At day 19, we observed the transformation of the structure of the tumor (fig. 1J). In fact, cluster 12 was replaced partially by cluster 13. On the other hand, the tumor occupied almost the entire hemisphere as visualized on the tissue of section (fig. 1I).

Fig. 3 shows class average spectra associated to normal brain structures and tumor development. The lipids spectra contain a large proportion of methyl, methylene and carbonyl bands in the region 2600-3700 cm^{-1}. The bands at 2852 cm^{-1} and 2924 cm^{-1} were due to the symmetric CH_2 stretching mode of the membrane lipid which is directly related to the lipid acyl, primarily saturated, chains. The band at 2956 cm^{-1} is associated to asymmetric CH_3 stretching mode of the methyl group and less contribution of proteins. The =C–H stretching bands due to unsaturated acyl chains are found at 3014 cm^{-1}. The bands at 3292 cm^{-1} and 3080 cm^{-1} were linked to the Amide A (mainly N–H stretching) and Amide B (N–H

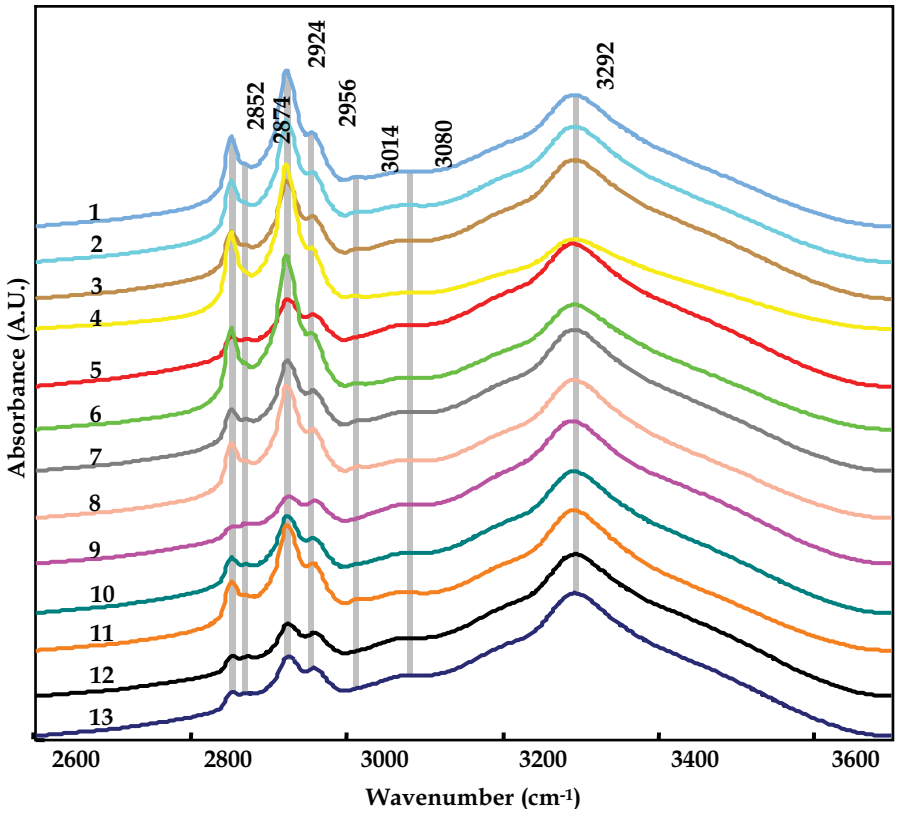

Fig. 3. Representative cluster mean FTIR spectra extracted from pseudocolor maps. Cluster averaged spectra were obtained by meaning absorbance spectra associated to each group. 13 models describing normal and glioma brain development. Each cluster averaged spectrum assigned to one class was plotted with the same color than in pseudo-color map

stretching) of proteins respectively. The band at 2874 cm^{-1} was related mainly to the symmetric stretch of proteins. The changes in frequencies, intensities and band shapes of these bands may provide further information about the structural changes associated with malignancy. In the malignant tissues, i) the intensity of the symmetric CH_2 band decreased compared to the corresponding bands in normal brain structures (white matter and grey matter) and ii) the band ratio 3292/2852 cm^{-1} was higher in the glioma tumor and reduced in the normal brain tissues. Indeed, the intensity ratio 2924/2956 cm^{-1} was higher in the spectra associated to white matter and decreased from grey matter to C6 glioma tumors. Band 2874 cm^{-1} became better resolved in the spectra of malignant tissues because of diminished intensities of CH_2 bands in this region. Therefore, the largest variances from spectra to spectra in IR spectroscopic maps of normal tissue were assigned to spectral contributions of lipids reflecting cell differentiation. This result confirms that the development of tumor was characterized by a reduction in total lipid content. This reduction was also observed in the invasive area (clusters 5 and 7), which is composed of healthy and tumoral cells. This result is in agreement with those obtained in brain diseases (Krafft et al., 2006; Kneipp et al., 2000).

This lipid reduction in malignant tissues could be related to the fast growth of tumor cells which need more energy (Wang et al., 2003). Indeed, it is known that, in developing brain tumors, structural and functional cell changes take place in which lipids play a crucial role. Yet, qualitative and quantitative aspects of lipid changes in brain tumors of different degree of malignancy are still the subject of numerous studies (Steiner et al., 2003; Krafft et al., 2006; Campanella, 1992).

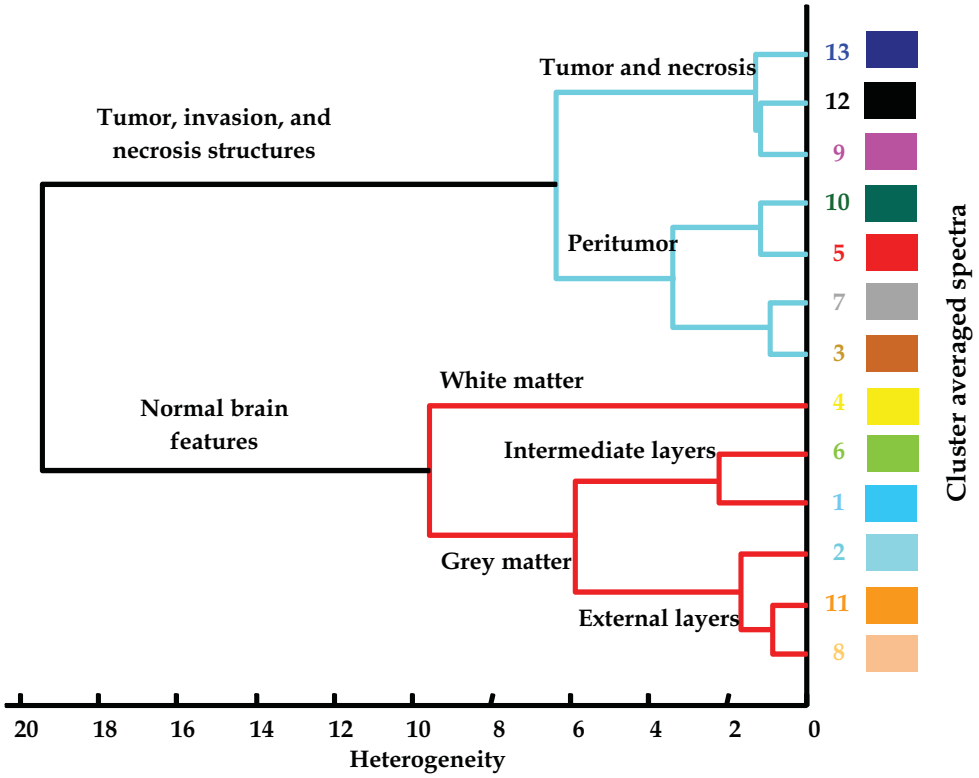

Fig. 4. Dendrogram obtained from hierarchical cluster analysis on spectral cluster averages associated to different tissue types. Heterogeneity represents the discriminating distance given by arbitrary units (au)

To distinguish between normal, tumor, and necrotic brain structures, cluster averaged spectra obtained from pseudo-color maps were input in the hierarchical cluster analysis using Ward's clustering algorithm and the square Euclidian distance measure. The result, as shown on the dendrogram in Fig. 4, showed a clear distinction between all normal and tumor brain structures. Indeed, the class related to normal brain structures was divided to two sub-clusters associated to white matter (clusters 4 corresponding to higher lipid content) and the second sub-cluster related to grey matter described by clusters 1 and 6 (intermediate cortex layers) and clusters 2, 8, and 11 (external cortex layers). We were also able to discriminate between glioma tumor (clusters 12, and 13) and necrosis (cluster 9) from peri-necrosis (clusters 3, 5, 7, and 10) in the second groups. In general, an increase in

malignancy is accompanied by a reduction in total lipids that involves all main classes of lipids found in plasma membranes (Campanella, 1992). Changes in lipid and in phospholipids contents, as seen in glioblastoma as compared with adjacent tissue, could indicate an evolution in the undergoing pathological process. This loss of lipids, correlated with demyelination, observed in different disorders, could be used as a spectroscopic marker. Increased levels of cholesterol esters (cholesterol oleate and linoleate) have also been reported in glioma tissue (Koljenovic et al., 2002). Koljenoviv et al. demonstrated that the difference between meningioma and dura is mainly related to lipids, cholesterol linoleate and linoleic acid levels. Steiner et al. studied the discriminating constituents between normal and tumoral tissues (astrocytoma and glioblastoma) by infrared spectroscopy (Steiner et al., 2003). They demonstrated that changes mainly arise from differences in lipid constituents. The potential use of lipid measurements for judging the stage, and hence the prognosis, of low grade tumors is suggested by the apparent gradual increase in lipid content over time. This increase, believed to be associated with necrosis, could thus be used in low grade tumors as an early marker of disease prior to the patient becoming symptomatic (Krafft et al., 2006; Koljenovic et al., 2005; Steiner et al., 2003). During tumor development, tissue composition and concentration of lipids decreased. Kraft et al. have investigated the lipid content of the white matter of human brain tissue using near infrared Raman spectroscopy (Krafft et al., 2005). They reported that the brain lipids can be divided into three principal classes: neutral lipids, phospholipids and sphingolipids.

3. Distribution of molecular changes in brain constituents associated to tumor growth and invasion

We have investigated the spatial distribution of molecular changes associated to C6 glioma progression using FT-IR micro-spectro-imaging in order to better understand the tissue transformation during carcinogenesis. Integrated intensity ratios bands were used in the region of 3700–2800 cm^{-1} to characterize differences between healthy and pathological brain. Maps of absorbance intensity ratios of bands in the region from 3000 to 2800 cm^{-1} due to CH_2 and CH_3 stretching vibrations (mainly due to membrane lipid which is directly related to the lipid acyl, primarily saturated) and those due to CH_2 and NH stretching vibrations (due to the protein-to-lipid ratios) were calculated and pseudo color maps scores were constructed (Fig. 5). These integrated absorbance intensity were correlated to molecular changes associated to tissue transformation. The comparison between the pseudo color scores maps and histological image shows that high scores described the white matter structures such as CC and CA (colorbar). These scores decreased in the grey matter and become null in the tumor tissues. This intensity ratio was correlated to myelin content. In fact, white matter presents important lipid content due to high myelin level. The concentration of myelin decreased from CC to cortex. In general, an increase in malignancy is accompanied by a reduction in total lipids that involves all main classes of lipids found in plasma membranes (Krafft et al., 2006). This loss of lipids was correlated with demyelination, observed in the scores maps associated to tumor. We have study the distribution of the intensity ratio 3292/2852 cm^{-1} corresponds to NH stretching vibration in proteins vs symmetric CH_2 stretching mode of the membrane lipid. The results show that high score value was related to tumor at days 7, 12, 15, and 19 days PI. These scores decreased from invasion zone to normal brain structures (white matter and grey matter). The common underlying effects of malignancy are changes in the constituents that lead to

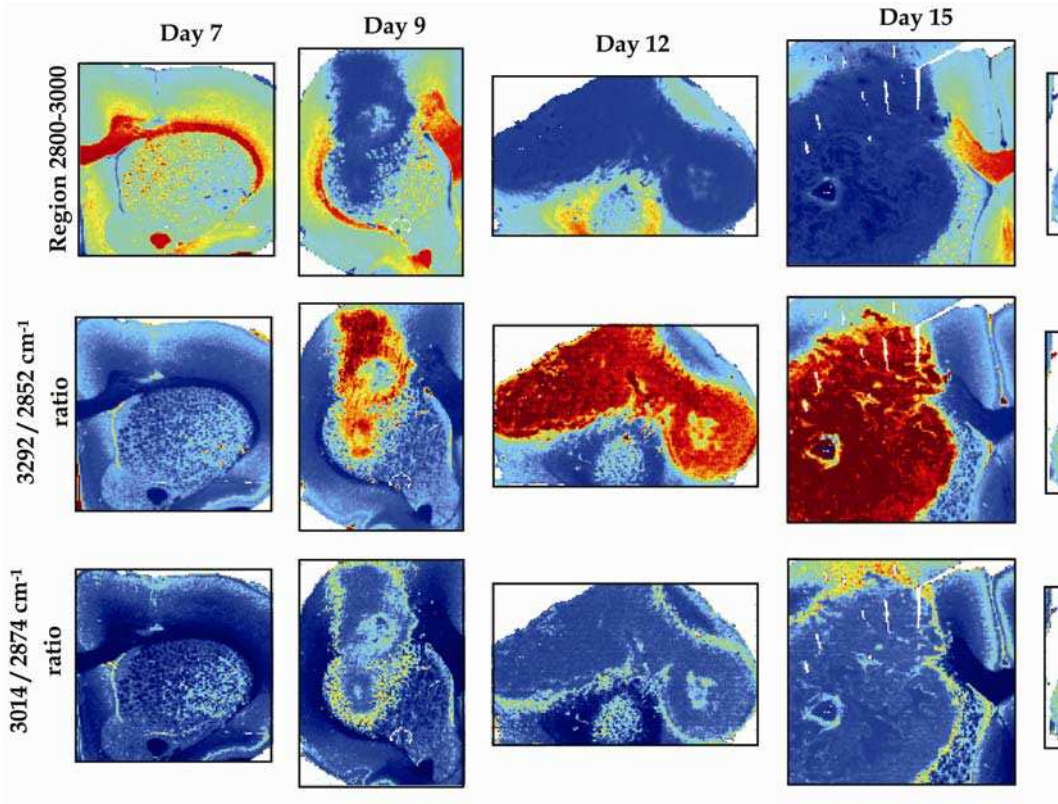

Fig. 5. Biochemical distribution of the changes in the molecular composition of tissues through the
Maps of absorbance intensity ratios of bands in the region from 3000 to 2800 cm^{-1} due to CH_2 and
(mainly due to membrane lipid which is directly related to the lipid acyl, primarily saturated) and
stretching vibrations (due to the protein-to-lipid ratio) were constructed and used to identify whic
be more potential indicators of such variations between normal and tumor development

an altered metabolism and biochemical composition in the malignant tissues. This study confirms the absorption intensity ratios were correlated with the histological state of the sample. Such a result may indicate the change of lipid and protein distribution in pathological tissues with respect to healthy one. There are some papers considering the pathological state of tissues by analysis of the changes in band intensities in the region from 3700 to 2800 cm^{-1}. Eckel et al. have analyzed breast cancer tissues (Eckel et al., 2001). They have considered the 3300 cm^{-1} band which corresponds to NH stretching vibration in proteins as a good criterion for distinguishing between non-cancerous and cancerous parts of tissue. Liu et al. applied IR absorption of human breast tissues in vitro and studied the CH stretching region of lipids and NH absorption region from 3600 to 2700 cm^{-1} (Liu et al., 2006). Gazi et al. used Synchrotron-FTIRM imaging to study prostate cancer cells and analyzed the distribution of lipid absorption intensities (CH_2 and CH_3) in the region from 3000 to 2800 cm^{-1} (Gazi et al., 2005) Krafft et al. have evaluated the usefulness of the lipid-to-protein ratio (2850/1655 cm^{-1}) as a spectroscopic marker to discriminate between normal and tumor tissue, as well as between low- and high-grade glioma tissues. They demonstrated that this ratio is maximal for normal brain tissue and decreases with the progression of the disease (Krafft et al., 2007). The intensity ratio 3014/2874 cm^{-1} was higher in the invasion zone and peritumor part of the necrosis and decreased in the tumor and normal brain tissues. This intensity ratio can be used to provide an objective method to delineate lesion margins that would reduce unnecessary tissue excisions.

4. Conclusion

This study demonstrated that FT-IRM imaging, with high spatially resolved morphological and biochemical information can be used as a diagnostic tool, complementary to histopathology in order to understand the molecular changes associated to C6 glioma progression. Cluster analysis allowed investigation of C6 glioma progression (from day 7 to day 19 post implantation). Different clusters in the FTIR images were correlated with features of the histopathological images such as white and grey matters, tumor, peritumor, and necrosis. Our results showed that 7 days after tumor implantation, FTIR investigations displayed a very small abnormal zone associated with the proliferation of C6 cells in the caudate putamen. From this day, rats developed solid and well-circumscribed tumors. Additionally, we have identified one peculiar structure all around the tumour. This structure was attributed to infiltrative events, such as peritumoral oedema observed during tumor development. The presence of necrotic areas was visible from day 15. In fact, the grade of malignancy and prognosis, in particular GBM multiforme, is based on the presence of necrosis. By combining intensity ratios of specific bands with imaging technique, we were able to take in account the variance due to the heterogeneity of brain tissues. We have monitored the changes in the intensity ratios of specific bands related to lipid and proteins. Our results reported that by correlating pseudocolor map scores with H&E staining it was possible to screen histological changes associated with tissue transformation. In fact, the integrated intensity in the 2800 to 3000 cm^{-1} spectral region described normal brain structures such as white matter (CC and CA) and some cortex layers (grey matter). The intensity decreased in the tumor tissues. Intensity ratio 3292/2852 cm^{-1} allowed the identification of tumor part of the tissue. The invasion zone was described by the 3014/2874 cm^{-1} ratio. These constituents can be used as spectroscopic markers for early detection of tissue abnormality and discrimination among normal, invasion, tumor and necrosis.

5. Acknowledgement

This work was supported by La Ligue de la Marne contre le Cancer, France.

6. References

Afanasyeva, N. I., Kolyakov, S.F., Artjushenko, S.G., Sokolov, V.V. & Frank, G.A. (1998). Minimally invasive and ex vivo diagnostics of breast cancer tissues by fiber optic evanescent wave Fourier transform IR (FEW-FT-IR) spectroscopy. *Proceedings of SPIE - The International Society for Optical Engineering*, pp. 140-146. 0277786X, San Jose, CA,

Amharref, N., Beljebbar, A., Dukic, S., Venteo, L., Schneider, L., Pluot, M., Vistelle, R.. & Manfait, M. (2006). Brain tissue characterisation by infrared imaging in a rat glioma model. *Biochim. Biophys. Acta*, Vol. 1758, No. 7, (07.2006) 892-899, ISSN 00052736

Amharref, N., Beljebbar, A., Dukic, S., Venteo, L., Schneider, L. Pluot, M., & Manfait, M. (2007). Discriminating healthy from tumor and necrosis tissue in rat brain tissue samples by Raman spectral imaging. *Biochim. Biophys. Acta*, Vol. 1768, No. 10, (10 2007) 2605-2615, ISSN 00052736.

Auer, R.N., Del Maestro, R.F., Anderson, R. (1981). A simple and reproducible experimental in vivo glioma model. *Can J Neurol Sci.,* Vol. 8, No. 4, (11 1981), pp. 325-331, ISSN 0317-1671.

Barker, F.G., Davis, R.L., Chang, S.M., & Prados, M.D. (1996). Necrosis as a prognostic factor in glioblastoma multiforme. *Cancer*, Vol. 77, No. 6, (03 1996), 1161-1166, ISSN 0008543X.

Barth, R.F. (1998). Rat brain tumor models in experimental neuro-oncology: the 9L, C6, T9, F98, RG2 (D74), RT-2 and CNS-1 gliomas. *Neurooncol*., Vol. 36, No. 1, (01 1998), pp. 91-102, ISSN 0167-594X.

Bates, J.B. (1976). Fourier transform infrared spectroscopy. *Science,* Vol. 9, No. 191, 4222, (01.1976), pp. 31-37, ISSN 00368075

Beljebbar, A., Amharref, N., Lévèques, A., Dukic, S., Venteo, L., Schneider, L., Pluot, M., & Manfait, M. (2008). Modeling and quantifying biochemical changes in C6 tumor gliomas by Fourier transform infrared imaging. *Anal. Chem*., Vol. 15, No 80, (11.2008), pp. 8406-8415, ISSN 00032700

Bernstein, J.J., Laws, E.R. Jr, Levine, K.V., Wood, L.R., Tadvalkar, G., Goldberg, W.J. (1991). C6 glioma-astrocytoma cell and fetal astrocyte migration into artificial basement membrane: a permissive substrate for neural tumors but not fetal astrocytes. *Neurosurgery*, Vol. 28, No. 5, (5 1991), pp. 652-658, ISSN 0148-396X.

Burwell, R.D. (2001). Borders and cytoarchitecture of the perirhinal and postrhinal cortices in the rat, *J. comparative neurol.*. Vol. 437, No. 1, (08 2001), pp. 17-41, ISSN 00219967.

Campanella, R., (1992). Membrane lipids modifications in human gliomas of different degree of malignancy. *J. Neurosurg. Sci.,* vol. 36, No. 1, (1992), pp. 11–25, ISSN 00264881.

Cherayil, G.D.& Scaria, K.S. (1970). Thin-layer chromatography of tissue lipids without extraction. J. Lipid Res., Vol. 11, No. 4, (07 1970), pp. 378-381, ISSN 00222275.

Chicoine, M.R., & Silbergeld, D.L. (1995). Invading C6 glioma cells maintaining tumorigenicity. *J Neurosurg* Vol. 83, No. 4, (10 1995), pp. 665-671, ISSN 0022-3085.

Ci, Y., Gao, T., Feng, J., & Guo Z. (1999). Fourier transform infrared spectroscopic characterization of human breast tissue: implications for breast cancer diagnosis. *Applied Spectrosc.*, Vol. 53, No. 3, (03.1999), pp. 312–315, ISSN 00037028

Cohenford, M.A. & Rigas B. (1998). Cytologically normal cells from neoplastic cervical samples display extensive structural abnormalities on IR spectroscopy: implications for tumor biology. *Proc. Natl. Acad. Sci. U S A.,* Vol. 95, No. 26, (12.1998), pp. 15327–15332, ISSN 00278424

Diem, M., Boydston-White, S. & Chiriboga, L. (1999). Infrared spectroscopy of cells and tissues: shining light onto a novel subject. *Appl. Spectrosc.*, Vol. 53, No. 4, pp. 148-161, ISSN 00037028

Eckel, R., Huo, H., Guan, H.W., Hu, X., Che X., & Huang W.D. (2001).Characteristic infrared spectroscopic patterns in the protein bands of human breast cancer tissue. *Vib. Spectrosc.,* Vol. 27, No. 2,, (12 2001), pp. 165–173, ISSN 09242031.

Fernandez, D.C., Bhargava, R., Hewitt, S.M.& Levin, I.W. (2005). Infrared spectroscopic imaging for histopathologic recognition. *Nature Biotechnology,* Vol. 23, No. 4, pp. 469-474, ISSN 10870156

Franck, P., Nabet, P. & Dousset, B. (1998). Applications of infrared spectroscopy to medical biology. *Cell. Mol. Biol.*, Vol. 44, No. 2, (03.1998), pp. 273- 275, ISSN 01455680

Gazi, E., Dwyer, J., Lockyer, N.P., Miyan, J., Gardner, P., Hart, C.A., Brown M.D., & Clarke N.W. (2005). A study of cytokinetic and motile prostate cancer cells using synchrotron-based FTIR microspectroscopic imaging. *Vib. Spectrosc.*, Vol. 38, No. 1-2, (07 2005), pp. 193–201, ISSN 09242031.

Goodacre, R., Vaidyanathan, S., Dunn, W.B., Harrigan, G.G. & Kell, D.B. (2004). Metabolomics by numbers: Acquiring and understanding global metabolite data, *Trends Biotechnol.*, Vol. 22, No. 5, (05.2004), pp. 245–252, ISSN 01677799.

Grobben, B, De Deyn, P.P., & Slegers, H. (2002). Rat C6 glioma as experimental model system for the study of glioblastoma growth and invasion. *Cell Tissue Res.*, Vol. 310, No. 3,, pp. 257-270, ISSN 0302766X.

Jackson, M., Ramjiawan, B., Hewko, M., & Mantsch, H.H.. (1998). Infrared microscopic functional group mapping and spectral clustering analysis of hypercholesteramic rabbit liver. *Cell. Mol. Biol.*, Vol. 44, No. 1, (02.1998), pp. 89–98, ISSN 01455680

Kleihues, P., Burger, P.C ., Scheithauer, B.W. (1993). The new WHO classification of brain tumours. *Brain Pathol.*, Vol. 3, No. 3, (03 1993), pp. 255-68, ISSN 10156305.

Kneipp, J., Lasch, P., Baldauf, E., Beekes, M., & D. Naumann, (2000). Detection of pathological molecular alterations in scrapie-infected hamster brain by Fourier transform infrared spectroscopy. *Biochim. Biophys. Acta*, Vol. 1501, No. 2-3, (06 2000), pp. 189-199, ISSN 09254439.

Koljenovic, S., Choo-Smith, L.P., Bakker Schut, T.C., Kros, J.M., van den Berge, H.J., & Puppels, G. (2002). Discriminating vital tumor from necrotic tissue in human glioblastoma tissue samples by Raman spectroscopy. *Lab. Invest.*, Vol. 82, No. 100, (10 2002) pp. 1265-1277, ISSN 00236837.

Koljenovic, S., Schut, T.B., Vincent, A., Kros, J.M., Puppels, G.J. (2005). Detection of meningioma in dura mater by Raman spectroscopy. *Anal. Chem.*, Vol. 77, No. 24, (12 2005), pp. 7958-7965, ISSN 00032700.

Krafft, C., Neudert, L., Simat, T., & Salzer, R. (2005). Near infrared Raman spectra of human brain lipids. *Spectrochim. Acta (Part A),* Vol. 61, No. 7, (05 2005), pp. 1529-1535, ISSN 13861425.

Krafft, C., Sobottka, S.B., Geiger, K.D., Schackert, G., & Salzer, R. (2007). Classification of malignant gliomas by infrared spectroscopic imaging and linear discriminant analysis. *Anal. Bioanal. Chem.*, Vol. 387, No. 5, (03 2007), pp. 1669-1677, ISSN 16182642

Krafft, C., Sobottka, S.B., Schackert, G., & Salzer R. (2006). Raman and infrared spectroscopic mapping of human primary intracranial tumors: A comparative study. *J. Raman Spectrosc.*, Vol. 37, No. 1-3, (01 2006), pp. 367-375, ISSN 03770486.

Krafft, C., Thummler, K., Sobottka, S.B., Schackert, G., & Salzer, R. (2006). Classification of malignant gliomas by infrared spectroscopy and linear discriminant analysis. *Biopolymers*, Vol. 82, No. 4, (07 2006), pp. 301-305, ISSN 00063525

Lasch, P & Naumann D. (1998). FT-IR microspectroscopic imaging of human carcinoma thin sections based on pattern recognition techniques. *Cell. Mol. Biol.*, Vol. 44, No. 1, (02.1998), pp. 189–202, ISSN 01455680.

Lasch, P., Haensch, W., Naumann, D., & Diem, M. (2004). Imaging of colorectal adenocarcinoma using FT-IR microspectroscopy and cluster analysis. *Biochim Biophys Acta., Vol.* 1688, No. 2, (03.2004), pp. 176–186, ISSN 09254439.

Laws, E.R. Jr & Shaffrey, M.E. (1999). The inherent invasiveness of cerebral gliomas: Implications for clinical management. *Int. J. Dev. Neurosci.,* Vol. 17, No. 5-6, (08 1999), pp. 413-420, ISSN 07365748

Levin, I.W. & Bhargava, R. (2005). Fourier transform infrared vibrational spectroscopic imaging: Integrating microscopy and molecular recognition. *Annu. Rev. Phys. Chem.*, Vol. 56, pp. 429-474, ISSN 0066426X

Li, Q.B., Sun, X.J., Xu, Y.Z., Yang, L.M., Zhang, Y.F., Weng, S.F., Shi, J.S & Wu, J.G (2005). Diagnosis of gastric inflammation and malignancy in endoscopic biopsies based on Fourier transform infrared spectroscopy. *Clin. Chem.*, vol. 51, No. 2, (02.2005), pp 346–350, ISSN 00099147

Liu, C., Zhang, Y., Yan, X., Zhang, X., Li, C., Yang W., & Shi, D. (2006). SR-FTIR spectroscopic preliminary findings of non-cancerous. J. Lumin., Vol. 119–120, SPEC, (07 2006), pp. 132–136, ISSN 00222313.

Mansfield, J.R., McIntosh, K., Crowson, A.N., Mantsch, H.H. & Jackson, M. (1999). LDA-guided search engine for the non-subjective analysis of infrared microspectroscopic maps. *Appl. Spectrosc., Vol.* 53, No. 11, (11.1999), pp. 1323–1330, ISSN 00037028.

Mansfield, J.R., Sowa, M.G., Scarth, G.B., Somorjai, R.L. & Mantsch, H.H. (1997). Analysis of spectroscopic imaging data by fuzzy C-means clustering. *Anal. Chem.*, Vol. 69, No. 16, (08.1997), pp. 3370–3374, ISSN 00032700.

Mohlenhoff, B., Romeo, M., Diem, M., & Wood, B.R. (2005). Mie-type scattering and non-Beer-Lambert absorption behaviour of human cells in infrared microspectroscopy. *Biophys J.,* Vol. 88, No. 5, (05.2005), pp. 3635–3640, ISSN 00063495.

Mourant, J. R., Yamada, Y.R. Carpenter, S., Dominique, L.R. & Freyer, J.P. (2003). FTIR spectroscopy demonstrates biochemical differences in mammalian cell cultures at different growth stages. *Biophys. J.*, Vol. 85, No. 3, (09.2003) 1938–1947, ISSN 00063495.

Nagano, N., Sasaki, H., Aoyagi, M., & Hirakawa, K. (1993). Invasion of experimental rat brain tumor: early morphological changes following microinjection of C6 glioma cells. *Acta Neuropathol*., Vol. 86, No. 2, (1993), pp. 117-125, ISSN 00016322.

Parker, F. S., (1971). *Application of infrared spectroscopy in biochemistry, biology and medicine* Plenum, New York.

Petibois, C. & Déléris, G. (2006). Chemical mapping of tumor progression by FT-IR imaging: towards molecular histopathology. *Trends in Biotechnology*, Vol. 24, No. 10, (08.2006), pp. 455-462, ISSN 01677799

Rigas, B., Morgello, S., Goldman, I., & Wong, P. (1990). Human colorectal cancers display abnormal Fourier-transform infrared spectra. *Proc. Natl. Acad. Sci. USA*, Vol. 87, No. 20, (10.1990), pp. 8140–8144, ISSN 00278424

San-Galli, F, Vrignaud, P., Robert, J., Coindre, J.M., Cohadon, F. (1989). Assessment of the experimental model of transplanted C6 glioblastoma in Wistar rats. *J. Neurooncol*., Vol. 7, No. 3, (9 1989), pp. 299-304, ISSN 0167594X.

Savitzky, A. & Golay, M.J.E. (1964). Smoothing and differentiation of data by simplified least squares procedures. *Anal. Chem*., Vol. 36, No. 8, (08 1964), pp. 1627-1639

Steiner, A., Shaw, G., Choo-Smith, L.P., Schackert, G., Steller, W., Abuid, H.M., & Salzer, R. (2003). Distinguishing and grading human gliomas by infrared spectroscopy. *Biopolymers*, Vol. 72, No. 6, (2003), pp. 464-471, ISSN 00063525.

Wang, J.S., Shi, J.S., Xu, Y.Z., Duan, X.Y., Zhang, L., Wang, J., Yang, L.M., Weng, S.F., & Wu, J.G. (2003). FT-IR spectroscopic analysis of normal and cancerous tissues of esophagus. *World J. Gastroenterol*., Vol. 9, No. 9, (09 2003), pp. 1897-1899, ISSN 10079327.

Wong, P.T., Wong, R.K., Caputo, T.A., Godwin, T.A. & Rigas, B. (1991). Infrared spectroscopy of exfoliated human cervical cells: Evidence of extensive structural changes during carcinogenesis. *Proc. Natl. Acad. Sci. USA*, Vol. 88, No. 24, (12.1991), pp. 10988–10992, ISSN 00278424

Yano, K., Ohoshima, S., Gotou, Y., Kumaido, K., Moriguchi, T.& Katayama H. (2000). Direct measurement of human lung cancerous and noncancerous tissues by Fourier transform infrared microscopy: can an infrared microscope be used as a clinical tool? *Anal. Biochem.* Vol. 287, No. 2, (12.2000), pp. 218–225, ISSN 00032697

Zhang, L., Small, G.W., Haka, A.S., Kidder, L.H., & Lewis, E.N. (2003). Classification of Fourier transform infrared microspectroscopic imaging data of human breast cells by cluster analysis and artificial neural networks. *Appl. Spectrosc*., Vol. 57, No. 1, (01.2003), pp. 14–22, ISSN 00037028.

Fourier Transforms - New Analytical Approaches and FTIR Strategies

Edited by Prof. Goran Nikolic

ISBN 978-953-307-232-6
Hard cover, 520 pages
Publisher InTech
Published online 01, April, 2011
Published in print edition April, 2011

New analytical strategies and techniques are necessary to meet requirements of modern technologies and new materials. In this sense, this book provides a thorough review of current analytical approaches, industrial practices, and strategies in Fourier transform application.

How to reference

In order to correctly reference this scholarly work, feel free to copy and paste the following:

Beljebbar A. and Manfait M. (2011). Fourier Transform Infrared Microspectroscopy for Cancer Diagnostic of C6 Glioma on Animal Model, Fourier Transforms - New Analytical Approaches and FTIR Strategies, Prof. Goran Nikolic (Ed.), ISBN: 978-953-307-232-6, InTech, Available from: http://www.intechopen.com/books/fourier-transforms-new-analytical-approaches-and-ftir-strategies/fourier-transform-infrared-microspectroscopy-for-cancer-diagnostic-of-c6-glioma-on-animal-model

INTECH
open science | open minds

InTech Europe
University Campus STeP Ri
Slavka Krautzeka 83/A
51000 Rijeka, Croatia
Phone: +385 (51) 770 447
Fax: +385 (51) 686 166
www.intechopen.com

InTech China
Unit 405, Office Block, Hotel Equatorial Shanghai
No.65, Yan An Road (West), Shanghai, 200040, China
中国上海市延安西路65号上海国际贵都大饭店办公楼405单元
Phone: +86-21-62489820
Fax: +86-21-62489821